


## Article

# Oxidation-Induced and Hydrothermal-Assisted Template-Free Synthesis of Mesoporous CeO<sub>2</sub> for Adsorption of Acid Orange 7

Yaohui Xu<sup>1</sup> and Zhao Ding<sup>2,\*</sup> 

<sup>1</sup> Laboratory for Functional Materials, School of New Energy Materials and Chemistry, Leshan Normal University, Leshan 614004, China; xyh1986@lsnu.edu.cn

<sup>2</sup> College of Materials Science and Engineering, National Engineering Research Center for Magnesium Alloys, Chongqing University, Chongqing 400044, China

\* Correspondence: zhaoding@cqu.edu.cn

**Abstract:** Hydrogen peroxide (H<sub>2</sub>O<sub>2</sub>), an accessible and eco-friendly oxidant, was employed for the template-free hydrothermal synthesis of mesoporous CeO<sub>2</sub> based on a cerium carbonate precursor (Ce<sub>2</sub>(CO<sub>3</sub>)<sub>3</sub>•xH<sub>2</sub>O). Its microstructure and physicochemical properties were characterized by XRD, TEM and N<sub>2</sub> sorption techniques. The formation of the CeO<sub>2</sub> phase with a porous structure was strongly dependent on the presence of H<sub>2</sub>O<sub>2</sub>, while the values of the BET surface area, pore diameter and pore volume of CeO<sub>2</sub> were generally related to the amount of H<sub>2</sub>O<sub>2</sub> in the template-free hydrothermal synthesis. The BET surface area and pore volume of the mesoporous CeO<sub>2</sub> synthesized hydrothermally at 180 °C with 10 mL H<sub>2</sub>O<sub>2</sub> were 112.8 m<sup>2</sup>/g and 0.1436 cm<sup>3</sup>/g, respectively. The adsorption process had basically finished within 30 min, and the maximum adsorption efficiency within 30 min was 99.8% for the mesoporous CeO<sub>2</sub> synthesized hydrothermally at 140 °C with 10 mL, when the initial AO7 concentration was 120 mg/L without pH preadjustment. The experimental data of AO7 adsorption were analyzed using the Langmuir and Freundlich isotherm modes. Moreover, the mesoporous CeO<sub>2</sub> synthesized at 140 °C with 10 mL H<sub>2</sub>O<sub>2</sub> was regenerated in successive adsorption–desorption cycles eight times without significant loss in adsorption capacity, suggesting that the as-synthesized mesoporous CeO<sub>2</sub> in this work was suitable as an adsorbent for the efficient adsorption of AO7 dye from an aqueous solution.

**Keywords:** CeO<sub>2</sub>; mesoporous; template-free; hydrothermal; adsorption; azo dye



**Citation:** Xu, Y.; Ding, Z. Oxidation-Induced and Hydrothermal-Assisted Template-Free Synthesis of Mesoporous CeO<sub>2</sub> for Adsorption of Acid Orange 7. *Materials* **2022**, *15*, 5209. <https://doi.org/10.3390/ma15155209>

Academic Editor: Carlos Javier Duran-Valle

Received: 2 July 2022

Accepted: 26 July 2022

Published: 27 July 2022

**Publisher's Note:** MDPI stays neutral with regard to jurisdictional claims in published maps and institutional affiliations.



**Copyright:** © 2022 by the authors. Licensee MDPI, Basel, Switzerland. This article is an open access article distributed under the terms and conditions of the Creative Commons Attribution (CC BY) license (<https://creativecommons.org/licenses/by/4.0/>).

## 1. Introduction

With the widespread use of various dyes, numerous dyes have been released into the environment in the process of the production and use of these dyes. Most dyes are extremely stable, and it is difficult for them to undergo natural degradation [1–3]. After entering a water environment, the chromaticity of the contaminated water is caused, which can affect the amount of incident light and the normal life activities of the aquatic animals and plants, and thus destruct the ecological balance of water. More severely, many dyes have carcinogenic and teratogenic effects because of their toxicity; they can directly or indirectly affect the health of the organism through the food chain [4–7]. Of today's different groups of dyes, azo dyes are the most varied synthetic dyes, accounting for 80% of total organic dye products. The azo dye wastewater is recognized as an obstinate organic wastewater because of its stable chemical structure [8]. Therefore, how to get rid of azo dye pollution from wastewater has been attracting significant attention. So far, numerous technical and engineering approaches have been engaged to treat azo dye wastewater, such as the adsorption method using activated carbon [9], membrane separation technology [10], magnetic separation technology [11], the chemical oxidation method [12] and the biological method [13]. Among these techniques, adsorption using a suitable adsorbent is an alternative procedure and exhibits the best results [14]. Meanwhile, ceria (CeO<sub>2</sub>) with a

mesoporous structure is a promising candidate for the removal of dye because of its high BET surface ( $S_{\text{BET}}$ ), well-defined pore topology and special surface states [15,16].

At present, most of the synthesis of  $\text{CeO}_2$  with porous structures involves the use of a series of soft or hard templates, and these templates must be sacrificed by subsequent dissolution using appropriate chemical reagents or decomposition by heat treatment [17–19]. For example, Jiang et al. [20] synthesized mesoporous  $\text{CeO}_2$  ( $S_{\text{BET}} = 150.8 \text{ m}^2/\text{g}$ ) using the pre-synthesized SBA-15 molecular structure as a template. The binary composite material ( $\text{CeO}_2/\text{SBA-15}$ ) was first synthesized hydrothermally at  $500 \text{ }^\circ\text{C}$  for 2 h. The as-synthesized  $\text{CeO}_2/\text{SBA-15}$  was added into 30 mL NaOH solution (10 mol/L) and stirred at  $100 \text{ }^\circ\text{C}$  for 48 h. After that, the precipitates were rinsed with water to a pH of 7. The above steps were repeated two to three times, and finally the mesoporous  $\text{CeO}_2$  was obtained. Fu et al. [21] fabricated mesoporous  $\text{CeO}_2$  ( $S_{\text{BET}} = 107.9 \text{ m}^2/\text{g}$ ) by the KIT-6-templating strategy using the ordered mesoporous silica (KIT-6) as a template. The mixture of KIT-6 and  $\text{Ce}(\text{NO}_3)_3 \cdot 6\text{H}_2\text{O}$  was calcined at  $600 \text{ }^\circ\text{C}$  for 6 h, and the as-obtained powders were twice treated in a hot ( $60 \text{ }^\circ\text{C}$ ) NaOH solution (2.0 mol/L) for the removal of the Si template. Recently, Li et al. [22] synthesized mono-dispersed hybrid microspheres composed of mesoporous  $\text{CeO}_2$  ( $S_{\text{BET}} = 67.2 \text{ m}^2/\text{g}$ ) by the hydrothermal approach and controlled calcination procedure. Glucose and acrylamide were used as templates during the hydrothermal process, and the precursor obtained by hydrothermal process was first calcined at  $600 \text{ }^\circ\text{C}$  for 6 h in an Ar atmosphere, and then calcined at  $500 \text{ }^\circ\text{C}$  for 4 h in air. Moreover, Zhao et al. [23] synthesized mesoporous  $\text{CeO}_2$  nanospheres ( $S_{\text{BET}} = 77.8 \text{ m}^2/\text{g}$ ) using the C-sphere template. The C-sphere@ $\text{CeO}_2$  precursor was first obtained by impregnation, combining the precipitation method with the prefabricated C-sphere as a template, and then 3D hollow mesoporous  $\text{CeO}_2$  nanospheres were obtained by calcining C-sphere@ $\text{CeO}_2$  precursor at  $550 \text{ }^\circ\text{C}$  for 2 h. Although their template method could synthesize mesoporous  $\text{CeO}_2$ , the soft or hard templates were essential, and thus either the procedure of dissolution or calcination was required to eliminate the soft or hard templates, but the energy consumption and costs were increased. Moreover, there have been limited reports for the direct and template-free synthesis of  $\text{CeO}_2$  with mesoporous structures until now [24–26]. Therefore, developing an effective, direct, and template-free synthetic strategy for mesoporous  $\text{CeO}_2$  is desirable. Despite their progresses in the template-free synthesis of mesoporous  $\text{CeO}_2$ , it is still challenging to further simplify the process, reduce costs and reduce energy consumption.

Herein, mesoporous  $\text{CeO}_2$  was synthesized by the hydrothermal process without adding any precipitants and template agents, and the subsequent high temperature roasting process was eliminated. So, the process has the advantages of simple operation, low cost and low energy consumption. Compared with previous research work in 2015 [27], this study used the off-the-shelf commercial  $\text{Ce}_2(\text{CO}_3)_3 \cdot x\text{H}_2\text{O}$  instead of pre-synthesized  $\text{Ce}_2(\text{CO}_3)_3 \cdot 8\text{H}_2\text{O}$  as the precursor, and studied the effects of the  $\text{H}_2\text{O}_2$  addition amount and reaction temperature on the  $S_{\text{BET}}$  and adsorption efficiency of acid orange 7 (AO7, azo dye). The cerium carbonate precursor ( $\text{Ce}_2(\text{CO}_3)_3 \cdot x\text{H}_2\text{O}$ ) was purchased and used as received without further purification. Significantly, hydrogen peroxide ( $\text{H}_2\text{O}_2$ ), an accessible and eco-friendly oxidant, was employed to achieve the phase transformation of  $\text{Ce}_2(\text{CO}_3)_3 \cdot x\text{H}_2\text{O}$  to  $\text{CeO}_2$  with a mesoporous structure under the cooperation of the following hydrothermal treatment. The microstructure and physicochemical properties of samples were characterized by XRD, TEM and  $\text{N}_2$  adsorption–desorption analyses. Moreover, the adsorption abilities of the as-synthesized mesoporous  $\text{CeO}_2$  were evaluated by adsorptive removal of AO7.

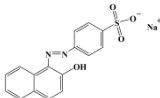
## 2. Experimental

### 2.1. Starting Materials

Cerium carbonate ( $\text{Ce}_2(\text{CO}_3)_3 \cdot x\text{H}_2\text{O}$ , 99.9%) and acid orange 7 (AO7, >97.0%) were supplied by Shanghai Maclin Biochemical Technology Co., Ltd. (Shanghai, China) and Tokyo Chemical Industry Co., Ltd. (Shanghai, China), respectively. The general characteristics of the AO7 dye are shown in Table 1. Hydrogen peroxide ( $\text{H}_2\text{O}_2$ ,  $\geq 30\%$ ) and ethanol

(≥99.7%) were supplied by Chengdu Kelong Chemical Co., Ltd. (Chengdu, China). All major chemicals were used as received without further purification, and distilled water was used in all experiments.

**Table 1.** General characteristics of AO7 dye.

Generic Name	Chemical Formula	Chemical Structure	Molecular Weight (g/mol)	Cas Number	$\lambda_{\max}$ (nm)	Appearance
Acid orange 7	$C_{16}H_{11}N_2NaO_4S$		350.3	633-96-5	484	Orange-red

## 2.2. Synthesis

$H_2O_2$  was selected as an oxidant to assist the phase transformation of  $Ce_2(CO_3)_3 \cdot xH_2O$  precursor to  $CeO_2$ , and the hydrothermal process was employed to synthesize the final product,  $CeO_2$  with a porous structure. Typically, 3 mmol  $Ce_2(CO_3)_3 \cdot xH_2O$  powders and the desired amount of  $H_2O_2$  (2, 5, 8, 10 and 15 mL) were mixed, and the solution was allowed to stand for 2 h. After that, the distilled water was added to make a final volume of 20 mL. The above solution with precipitate was decanted into a 50 mL Teflon-lined stainless steel autoclave and maintained for 24 h at a set temperature (120, 140, 160, 180 and 200 °C). Finally, the pale yellow powders were collected and washed with distilled water and ethanol, and dried under air at 60 °C for 24 h.

For comparison, a sample was synthesized following the same procedure as the control at 180 °C for 24 h but in the absence of  $H_2O_2$ .

## 2.3. Characterization

The phases of the samples were examined by X-ray diffraction (XRD, DX-2700). The morphologies and microstructures of samples were examined by transmission electron microscopy (TEM, JEM-2100F). Nitrogen ( $N_2$ ) adsorption–desorption isotherms of  $CeO_2$  samples were measured on Micromeritics ASAP2460, and their specific surface areas ( $S_{BET}$ ) were calculated by the Brunauer–Emmett–Teller (BET) method. The pore diameters and pore volumes were determined by Barrett–Joyner–Halenda (BJH) analysis.

## 2.4. Evaluation of Adsorption Capacity

AO7 is a typical azo dye that is widely used in textile industries because of its low cost and high solubility in water. AO7 is a toxic synthetic dye, and its poor degradability allows it to exist in the environment for a long time and then cause environmental pollution. So, the removal of AO7 dye from water and wastewater due to its detrimental effects is essential. In this work, the adsorption ability of porous  $CeO_2$  was evaluated by the adsorptive removal of AO7 dye from simulated wastewater. Typically, 0.2 g of the as-synthesized  $CeO_2$  was dispersed into 100 mL AO7 solution with an initial concentration of 120 mg/L, and the mixture was stirred using a vibrator (200 rpm). About 4 mL of the suspension was taken continually at regular intervals and centrifuged. The absorbance of supernatant at regular intervals ( $A_t$ , a.u.) was measured at the maximum absorption wavelength of 484 nm for AO7 dye using an ultraviolet spectrophotometer (Techcomp UV-2600), and the adsorption efficiency at this moment ( $E_t$ , %) was estimated as the following Equation (1):

$$E_t(\%) = \frac{A_0 - A_t}{A_0} \times 100 \quad (1)$$

where  $A_0$  is the initial absorbance value of AO7 dye solution ( $[AO7] = 120$  mg/L) at the  $\lambda_{\max}$  of 484 nm.

### 3. Results and Discussion

#### 3.1. Characterization of Mesoporous CeO<sub>2</sub>

The phases of all samples were detected by XRD analysis. Figure 1a shows the XRD patterns of commercial Ce<sub>2</sub>(CO<sub>3</sub>)<sub>3</sub>•xH<sub>2</sub>O powders. As shown in Figure 1a, the XRD pattern of commercial Ce<sub>2</sub>(CO<sub>3</sub>)<sub>3</sub>•xH<sub>2</sub>O was well indexed to the characteristic peaks of Ce<sub>2</sub>(CO<sub>3</sub>)<sub>3</sub>•8H<sub>2</sub>O (Orthorhombic; JCPDS no. 38-0377), revealing the major chemical composition was Ce<sub>2</sub>(CO<sub>3</sub>)<sub>3</sub>•8H<sub>2</sub>O. Furthermore, the diffraction peaks at the diffraction angle in the 2θ region of 36–80° were not matched to any substance from JCPDS standard cards, but its profile was similar to these previous reports on Ce<sub>2</sub>(CO<sub>3</sub>)<sub>3</sub>•8H<sub>2</sub>O [27,28]. Figure 1b shows the XRD pattern of the resulting precipitate synthesized hydrothermally at 180 °C for 24 h without adding H<sub>2</sub>O<sub>2</sub>. The major phase of the as-obtained precipitate was Ce(CO<sub>3</sub>)OH (Hexagonal; JCPDS no. 52-0352). It could be found that pure CeO<sub>2</sub> phase was not obtained hydrothermally in the absence of H<sub>2</sub>O<sub>2</sub>.

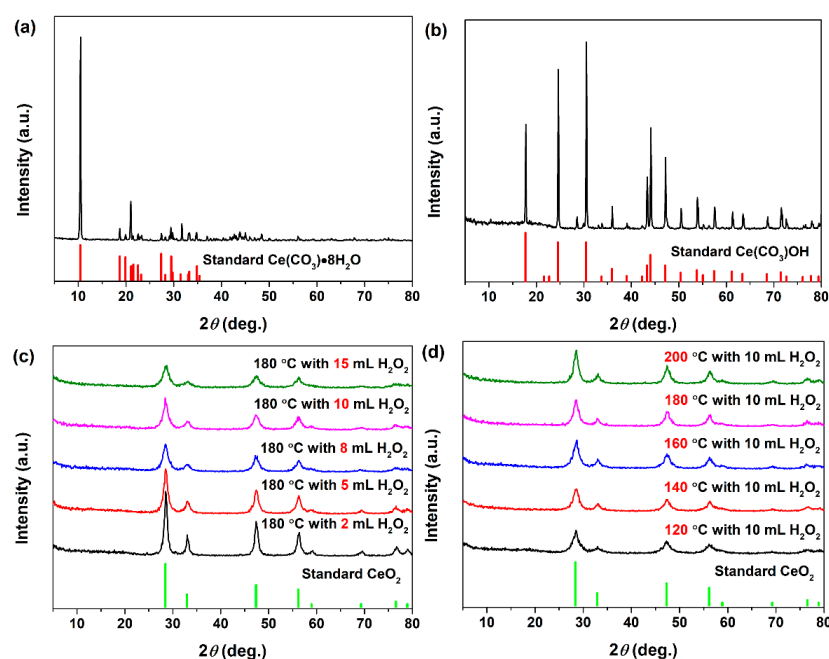


**Figure 1.** XRD patterns of (a) commercial Ce<sub>2</sub>(CO<sub>3</sub>)<sub>3</sub>•xH<sub>2</sub>O powders; The resulting precipitate synthesized hydrothermally (b) at 180 °C for 24 h without adding H<sub>2</sub>O<sub>2</sub>, (c) at 180 °C for 24 h with desired amounts H<sub>2</sub>O<sub>2</sub> of 2–15 mL, and (d) at a set temperature of 120–200 °C for 24 h with 10 mL H<sub>2</sub>O<sub>2</sub>.

Figure 1c,d show the resulting precipitates synthesized hydrothermally at 180 °C with a desired amount of H<sub>2</sub>O<sub>2</sub> and synthesized hydrothermally at a set temperature with 10 mL H<sub>2</sub>O<sub>2</sub>, respectively. As observed in Figure 1c,d, all broad peaks had a good match with the standard CeO<sub>2</sub> pattern (Cubic; JCPDS no. 34-0394), suggesting that the as-synthesized CeO<sub>2</sub> had a good crystallinity. Moreover, no additional phases for impurities were detected (such as Ce<sub>2</sub>(CO<sub>3</sub>)<sub>3</sub>•8H<sub>2</sub>O and Ce<sub>2</sub>(CO<sub>3</sub>)OH), which indicated that the single phase CeO<sub>2</sub> could be successfully obtained by hydrothermal process in the presence of H<sub>2</sub>O<sub>2</sub>. The FWHM (full width at half maximum) in Figure 1c showed obvious broadening phenomenon with the added volume of H<sub>2</sub>O<sub>2</sub> increased. The broadening phenomenon of FWHM implied that the grain sizes of CeO<sub>2</sub> decreased. In the formation process of the CeO<sub>2</sub> phase, the H<sub>2</sub>O<sub>2</sub> acts as an oxidant; their added volume directly affects the number of CeO<sub>2</sub> crystal nucleus, and then affects their grain size. From Figure 1d, no significant changes on FWHM were observed with the increase in the hydrothermal temperature from 120 to 200 °C, which could be due to the constant amount of H<sub>2</sub>O<sub>2</sub> (10 mL). The results showed that the addition amount of H<sub>2</sub>O<sub>2</sub> could affect the grain size of the CeO<sub>2</sub> final products. According to the above XRD results of the evolution process, a clear phase transformation from orthorhombic

$\text{Ce}_2(\text{CO}_3)_3 \cdot 8\text{H}_2\text{O}$  to cubic  $\text{CeO}_2$  with better crystallinity was observed, which could verify the mechanism involving the oxidation-assisted dissolution of  $\text{Ce}_2(\text{CO}_3)_3 \cdot x\text{H}_2\text{O}$  precursor followed by the formation of the  $\text{CeO}_2$  phase.

The morphologies, sizes and microstructures of commercial  $\text{Ce}_2(\text{CO}_3)_3 \cdot x\text{H}_2\text{O}$  precursor and  $\text{CeO}_2$  sample synthesized hydrothermally at 200 °C with 10 mL  $\text{H}_2\text{O}_2$  were measured by TEM analysis. As observed in Figure 2a, there were no uniform morphologies and uniform sizes for commercial  $\text{Ce}_2(\text{CO}_3)_3 \cdot x\text{H}_2\text{O}$  particles, and these particles were basically on the micron scale with smooth and compact surfaces. After hydrothermal treatment at 200 °C in the presence of  $\text{H}_2\text{O}_2$ , it was clearly observed that the as-obtained  $\text{CeO}_2$  particles consisted of aggregated nanoparticles with a mean diameter of about 4.5 nm, and the pores resulted from these aggregated nanoparticles (see Figure 2b). This is a preliminary indication that the oxidation-induced and hydrothermal-assisted template-free synthesis of porous  $\text{CeO}_2$  is viable.

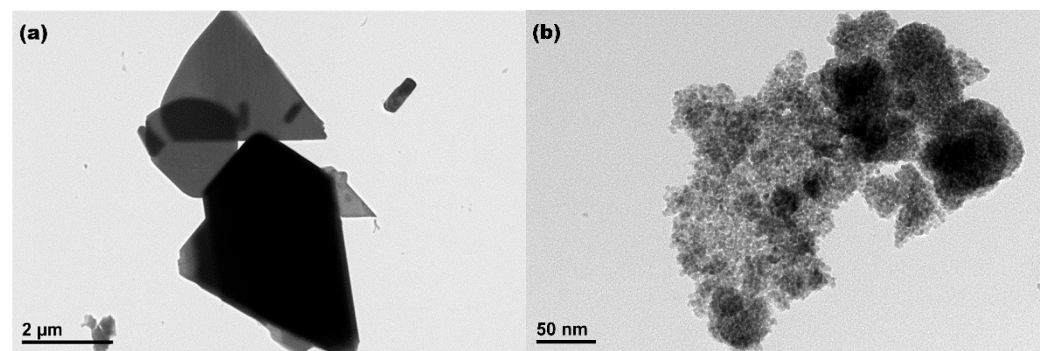


**Figure 2.** TEM images of (a) commercial  $\text{Ce}_2(\text{CO}_3)_3 \cdot x\text{H}_2\text{O}$  particles and (b)  $\text{CeO}_2$  sample synthesized hydrothermally at 200 °C for 24 h with 10 mL  $\text{H}_2\text{O}_2$ .

To further clarify the porous nature of the  $\text{CeO}_2$  final products,  $\text{N}_2$  adsorption–desorption experiments were conducted, and their  $S_{\text{BET}}$ , average pore sizes and pore volumes were estimated by  $\text{N}_2$  physisorption. Figure 3a,b show the  $\text{N}_2$  adsorption–desorption isotherms of the porous  $\text{CeO}_2$  synthesized hydrothermally at 180 °C with the desired amounts of  $\text{H}_2\text{O}_2$  of 2, 5 and 10 mL, and at a set temperature of 140 and 200 °C with 10 mL  $\text{H}_2\text{O}_2$ , respectively. From Figure 3, the similar hysteresis loops in the relative pressure ( $P/P_0$ ) range of 0.4–1.0 were observed, and these  $\text{N}_2$  adsorption–desorption isotherms were consistent with that of the mesoporous  $\text{CeO}_2$  reported in literatures [29–31], suggesting that these as-obtained  $\text{CeO}_2$  belonged to the mesoporous material [32].

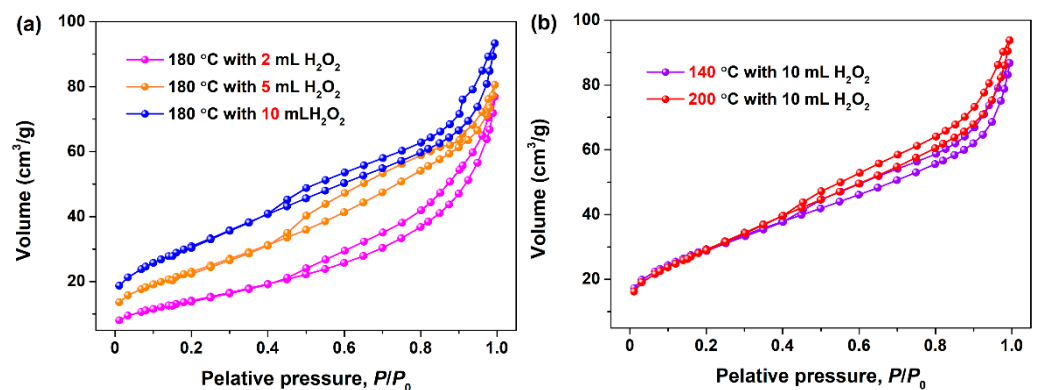


**Figure 3.**  $\text{N}_2$  adsorption–desorption isotherms of the mesoporous  $\text{CeO}_2$  synthesized hydrothermally (a) at 180 °C for 24 h with a desired amounts  $\text{H}_2\text{O}_2$  of 2, 5 and 10 mL, and (b) the mesoporous  $\text{CeO}_2$  synthesized hydrothermally at a set temperature of 140 and 200 °C for 24 h with 10 mL  $\text{H}_2\text{O}_2$ .

The determined values of  $S_{\text{BET}}$ , pore diameters and pore volumes are summarized in Table 2. As observed in Table 2, the  $S_{\text{BET}}$  of the mesoporous  $\text{CeO}_2$  powders synthesized hydrothermally at 180 °C with 2, 5 and 10 mL  $\text{H}_2\text{O}_2$  were determined as 52.5, 84.9 and 112.8  $\text{m}^2/\text{g}$ , respectively. These results implied that the amount of  $\text{H}_2\text{O}_2$  played a decisive role on the  $S_{\text{BET}}$ , as well as the pore diameter and pore volume. In other words, the more  $\text{H}_2\text{O}_2$  added, the larger these physicochemical parameters. Meanwhile, it can be found that the  $S_{\text{BET}}$  of the mesoporous  $\text{CeO}_2$  synthesized hydrothermally at 140, 180 and 200 °C with 10 mL  $\text{H}_2\text{O}_2$  were 107.0, 112.8 and 109.4  $\text{m}^2/\text{g}$ , respectively. It suggested that the hydrothermal temperature had little effect on the  $S_{\text{BET}}$  of the mesoporous  $\text{CeO}_2$  powders; however, it could affect the surface state of  $\text{CeO}_2$ , such as the empty 4f orbital of the cerium ion onto the  $\text{CeO}_2$  surface. Combining with the results of the XRD and TEM analyses, we could derive a conclusion that  $\text{H}_2\text{O}_2$  as an oxidant would play an important role in achieving phase transformation from  $\text{Ce}_2(\text{CO}_3)_3 \cdot x\text{H}_2\text{O}$  to  $\text{CeO}_2$  with a mesoporous structure; the addition amount of  $\text{H}_2\text{O}_2$  not only affects the grain size of  $\text{CeO}_2$ , but also determines the  $S_{\text{BET}}$ , pore diameters and pore volumes.

**Table 2.** Physicochemical properties of the mesoporous  $\text{CeO}_2$  synthesized hydrothermally at 180 °C for 24 h with a desired amounts  $\text{H}_2\text{O}_2$  of 2, 5 and 10 mL, and the mesoporous  $\text{CeO}_2$  synthesized hydrothermally at a set temperature of 140 and 200 °C for 24 h with 10 mL  $\text{H}_2\text{O}_2$ .

Synthesis Conditions	180 °C with Desired Amounts of $\text{H}_2\text{O}_2$			Different Temperaments with 10 mL $\text{H}_2\text{O}_2$	
	2 mL	5 mL	10 mL	140 °C	200 °C
$S_{\text{BET}}$ ( $\text{m}^2/\text{g}$ )	52.5	84.9	112.8	107.0	109.4
Pore diameter (nm)	8.95	5.81	5.09	4.98	5.28
Pore volume ( $\text{cm}^3/\text{g}$ )	0.1174	0.1234	0.1436	0.1332	0.1445

The specific surface areas were calculated by Brunauer–Emmett–Teller (BET) method (labeled as  $S_{\text{BET}}$ ), while the pore diameters and pore volumes were determined by Barrett–Joyner–Halenda (BJH) analysis.

### 3.2. Adsorption Characteristics

An anionic dye, AO7, was selected as the modal target to evaluate the adsorption performance of the as-synthesized mesoporous  $\text{CeO}_2$  powders without pH preadjustment. As shown in Figure 4a,b, the adsorption efficiencies within the first 10 min were surprisingly fast for all mesoporous  $\text{CeO}_2$  samples, above 60% of the AO7 was adsorbed, particularly the mesoporous  $\text{CeO}_2$  synthesized hydrothermally at 140 °C for 24 h with 10 mL  $\text{H}_2\text{O}_2$ , and the adsorption efficiency could reach 86.7%. Moreover, the adsorption efficiencies showed almost no significant changes after 30 min, indicating that the adsorption process had basically finished within 30 min. The maximum adsorption efficiency within 30 min was obtained with 99.8% for the mesoporous  $\text{CeO}_2$  synthesized hydrothermally at 140 °C with 10 mL  $\text{H}_2\text{O}_2$ . The fast and excellent adsorption of the mesoporous  $\text{CeO}_2$  for AO7 dye could be explained by the following three aspects. First, the as-synthesized  $\text{CeO}_2$  with mesoporous structures possessed high  $S_{\text{BET}}$ , which could provide for numerous sites for the adsorption of AO7, and then it increased their adsorption capacities. Second, the abundant pore structure of the mesoporous  $\text{CeO}_2$  was conducive to the transference of AO7 molecule toward the inside of this porous material, and then it increased the effectiveness of the contact between  $\text{CeO}_2$  adsorbent and AO7 adsorbate. Third, the strong adsorption toward AO7 may be attributed to the chelation interaction between the electron-rich groups (sulfonate group,  $\text{SO}_3^-$ ) of the AO7 molecule and the empty 4f orbital of cerium ion onto  $\text{CeO}_2$ .

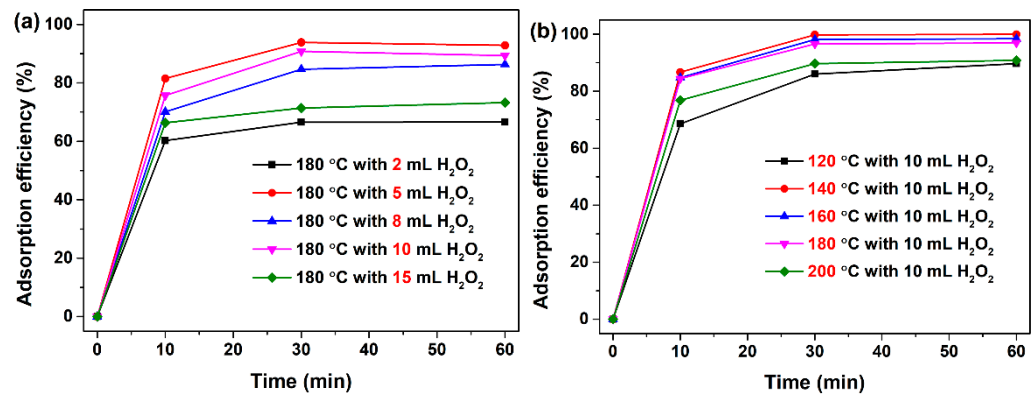


**Figure 4.** (a) Time-dependence of adsorption profiles of AO7 dye without pH pre-adjustment onto mesoporous CeO<sub>2</sub> synthesized hydrothermally at 180 °C for 24 h with a desired amount H<sub>2</sub>O<sub>2</sub> of 2–15 mL and (b) synthesized hydrothermally at a set temperature of 120–200 °C for 24 h with 10 mL H<sub>2</sub>O<sub>2</sub>. ([CeO<sub>2</sub>] = 2.0 g/L; [AO7] = 120 mg/L; V = 100 mL; distilled water; 200 rpm; room temperature).

Significantly, the mesoporous CeO<sub>2</sub> synthesized hydrothermally at 140 °C ( $S_{\text{BET}} = 107.0 \text{ m}^2/\text{g}$ ), 180 °C ( $S_{\text{BET}} = 112.8 \text{ m}^2/\text{g}$ ) and 200 °C ( $S_{\text{BET}} = 109.4 \text{ m}^2/\text{g}$ ) with 10 mL H<sub>2</sub>O<sub>2</sub> possessed similar  $S_{\text{BET}}$  (see Table 2); however, their adsorption efficiencies for AO7 within 30 min exhibited varying degrees of difference, and the values were 99.8%, 90.8% and 89.7%, respectively. Moreover, the mesoporous CeO<sub>2</sub> synthesized hydrothermally at 180 °C with 10 mL H<sub>2</sub>O<sub>2</sub> exhibited a maximum  $S_{\text{BET}}$  of 112.8 m<sup>2</sup>/g from Table 2; however, its adsorption efficiencies for AO7 within 30 min was not the maximum among all as-synthesized mesoporous CeO<sub>2</sub> powders. It indicates that the  $S_{\text{BET}}$  is not the only factor for the adsorption of AO7 dye onto mesoporous CeO<sub>2</sub> in this study, if any, including the CeO<sub>2</sub> surface state, such as the empty 4f orbital of cerium ion on the CeO<sub>2</sub> surface.

CeO<sub>2</sub> has selective adsorption for the anion dye with SO<sub>3</sub><sup>−</sup> groups, especially methyl orange (MO) and AO7 dyes [33,34]. In general, there are three coordination modes of SO<sub>3</sub><sup>−</sup> group: monodentate coordination, double dentate mononuclear coordination and bidentate biconuclear coordination. According to Deacon and Phillip’s theory and Bauer’s hypothesis, the wave-number distance between the peaks of asymmetric and symmetric vibration from the isolated SO<sub>3</sub><sup>−</sup> groups is larger than that of the adsorbed one, indicating that the SO<sub>3</sub><sup>−</sup> groups and Ce atoms form a tooth bridge integration [35]. According to the geometrical structure of AO7 molecule, when the adsorption reaction between AO7 and CeO<sub>2</sub> occurs, the two oxygen atoms on SO<sub>3</sub><sup>−</sup> group will coordinate with the two Ce atoms on CeO<sub>2</sub>, and the nitrogen atom from the azo bond (−N=N−) also will interact with the Ce atoms in the appropriate position [36].

To describe the interaction between the as-synthesized mesoporous CeO<sub>2</sub> and AO7 molecule and investigate the adsorption mechanism, the experimental data were analyzed by the Langmuir (Equation (2)) [37] and Freundlich [38] (Equation (3)) isotherm models, as shown in Figure 5a,b.

$$\frac{C_e}{q_e} = \frac{1}{q_m} C_e + \frac{1}{K_L q_m} \quad (2)$$

$$\log q_e = \frac{1}{n} \log C_e + \log K_F \quad (3)$$

where  $C_e$  (mg/L) and  $q_e$  (mg/g) are the concentration of AO7 solution and the amount of AO7 adsorbed per gram of CeO<sub>2</sub> at equilibrium, respectively.  $q_m$  (mg/g) is the maximum amount of AO7 molecule adsorbed per gram of CeO<sub>2</sub>.  $K_L$  and  $K_F$  are the Langmuir constant related to the energy of adsorption and the Freundlich constant related to the adsorption capacity, respectively.  $1/n$  is the heterogeneity factor, and  $n$  is the adsorption intensity.

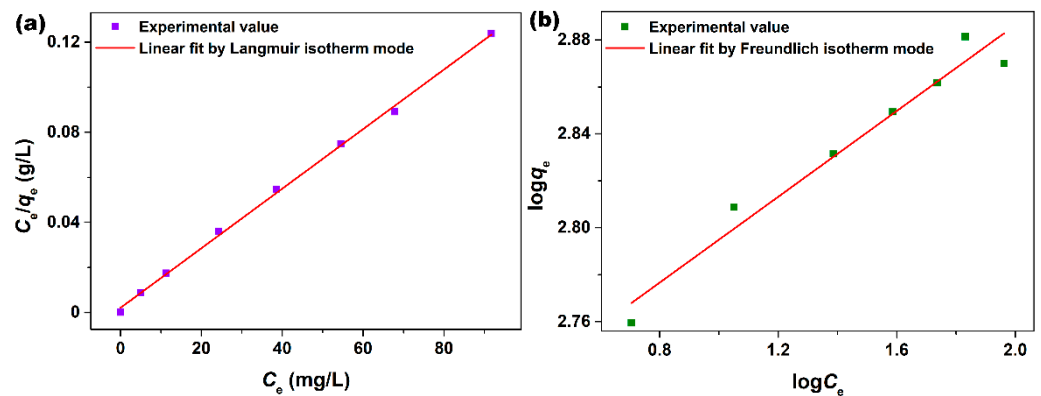


**Figure 5.** (a) Langmuir and (b) Freundlich linear fittings of AO7 molecule onto mesoporous CeO<sub>2</sub> synthesized hydrothermally at 140 °C for 24 h with 10 mL H<sub>2</sub>O<sub>2</sub>.

Figure 5a,b shows the Langmuir and Freundlich linear fittings of the experimental data of the adsorption of the AO7 molecule onto the mesoporous CeO<sub>2</sub> synthesized hydrothermally at 140 °C with 10 mL H<sub>2</sub>O<sub>2</sub>, and the relevant parameters calculated by Langmuir and Freundlich linear fittings are listed in Table 3. As observed in Figure 5a,b, it is found that the adsorption of the AO7 molecule onto the mesoporous CeO<sub>2</sub> can be described by both Langmuir and Freundlich isotherm models. However, the correlation coefficient ( $R^2$ ) for the Langmuir isotherm model ( $R^2 = 0.9985$ ) was much closer to 1.0 than that of the Freundlich isotherm model ( $R^2 = 0.9512$ ) from Table 3. According to the Langmuir isotherm model, the maximum amount of AO7 adsorbed on mesoporous CeO<sub>2</sub> could reach 757.6 mg/g at room temperature. Moreover, the Freundlich adsorption constant ( $n = 10.94$ ) related to the adsorption capacity was larger than 1, indicating that the adsorption intensity was favorable in the concentration range studied [39].

**Table 3.** Estimated parameters of Langmuir and Freundlich linear fittings for the adsorption of AO7 molecule onto mesoporous CeO<sub>2</sub> synthesized hydrothermally at 140 °C for 24 h with 10 mL H<sub>2</sub>O<sub>2</sub> at room temperature.

Langmuir Isotherm Model			Freundlich Isotherm Model		
$q_m$ (mg/g)	$K_L$	$R^2$	$n$	$K_F$	$R^2$
757.6	0.6256	0.9985	10.94	505.3	0.9512

Table 4 shows the maximum amount ( $q_m$ , mg/g) of AO7 molecule adsorbed per gram of various adsorbents from the recent literature [27,40–52]. By comparing the  $q_m$  of various adsorbent, we could see clearly that the adsorption capacity of the mesoporous CeO<sub>2</sub> synthesized hydrothermally at 140 °C with 10 mL H<sub>2</sub>O<sub>2</sub> in this work was among the very highest in these reported works in the literature. By noticing the  $S_{BET}$  and  $q_m$  of these adsorbents, it further indicated that the  $S_{BET}$  of the adsorbents was not the main factor determining their adsorption capacities. So, considering the unique electronic structure of CeO<sub>2</sub>, the adsorption mode of AO7 molecule on CeO<sub>2</sub> surface could be described as a Lewis acid-based reaction between the SO<sub>3</sub><sup>−</sup> groups of AO7 molecule and empty 4f orbital of cerium ion on CeO<sub>2</sub> surface, which eventually formed an inner-sphere complex. Therefore, both the addition amount of H<sub>2</sub>O<sub>2</sub> and the hydrothermal temperature affected the physicochemical state of the CeO<sub>2</sub> surface, and their joint action ultimately determined the adsorption capacity of mesoporous CeO<sub>2</sub> for AO7 dye.



**Table 4.** Recent literature on adsorbent development for the adsorption of AO7 dye.

Authors	Adsorbent Name	Sorption Conditions	$S_{BET}$ (m <sup>2</sup> /g)	$q_m$ (mg/g)
Pedro Silva [40]	Spent brewery grains (SBG)	30 °C	/	30.5
Hamzeh [41]	Canola stalks (CS)	25 °C; pH = 2.5	/	25.1
Ashori [42]	Soybean stalk (SS)	25 °C; pH = 2.0	/	17.5
Lin [43]	Iron oxide-loaded biochar (Fe-BC) from sorghum straw	25 °C; pH = 6.0; 180 rpm	216.6	59.3
Noorimotlagh [44]	Mesoporous activated carbon prepared from Iranian milk vetch	pH = 7.0	565	99.0
Lim [45]	Zeolite-activated carbon macrocomposite	Room temperature; pH = 7.0	84.7	0.19
Aber [46]	Powdered activated carbon	25 °C; pH = 2.8	/	440
Jia [47]	Multi-walled carbon nanotubes (MWCNTs)	pH = 7.0	~1800	47.7 ± 0.79
Nourmoradi [48]	Activated carbon coated with zinc oxide (AC-ZnO)	25 °C	/	66.2
Ghasemi [49]	Zeolitic imidazolate framework-8 (ZIF-8)	25 °C; pH = 6.0; 200 rpm	978	80.5
Zhou [50]	Fe <sub>3</sub> O <sub>4</sub> -poly(methacryloxyethyltrimethyl ammonium chloride) (Fe <sub>3</sub> O <sub>4</sub> -pDMC)	pH = 3.0; 150 rpm	35.7	270.3
Huo [51]	Nickel (II) oxide (NiO)	25 °C; pH = 5.5	251.8	178.6
Li [52]	Amine shield-introduced-released porous chitosan hydrogel beads (APCB)	30 °C; 150 rpm	/	2571.0 (pH = 2.0); 363.6 (pH = 4.0)
Xu [27]	Mesoporous CeO <sub>2</sub> synthesized based on integrating bottom-up and top-down routes in the previous report	25 °C; No pH preadjustment; 200 rpm	166.5	510.2
Xu	Mesoporous CeO <sub>2</sub> synthesized hydrothermally at 140 °C for 24 h with 10 mL H <sub>2</sub> O <sub>2</sub> in this work	Room temperature; No pH preadjustment; 200 rpm	107.0	757.6

### 3.3. Desorption and Reusability

Desorption of AO7 molecules from the adsorbed mesoporous CeO<sub>2</sub>, and the reusability of mesoporous CeO<sub>2</sub> are essential. In this experiment, 0.5 mol/L NaOH solution was used to desorb AO7 molecules from the mesoporous CeO<sub>2</sub> surface. The adsorption histogram in eight successive adsorption–desorption cycles is shown in Figure 6. It was clear that the adsorption efficiency could reach 98.4% in the first adsorption–desorption cycle. To examine the reproducibility of mesoporous CeO<sub>2</sub>, another seven adsorption–desorption cycles were performed. It can be found that the similar AO7 uptake capacity of the regenerated mesoporous CeO<sub>2</sub> only appeared to be slightly fading, and the adsorption efficiency for AO7 could maintain more than 92% after eight cycles. Due to the high recycling efficiency, the as-synthesized mesoporous CeO<sub>2</sub> in this work may be suitable as a promising adsorbent for water treatment or the removing of the AO7 dye.

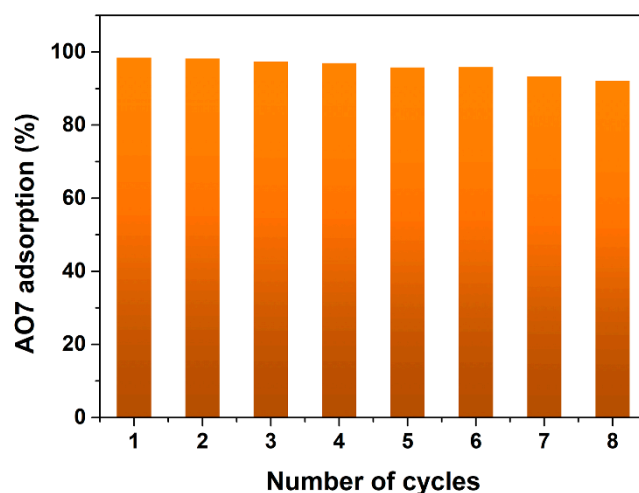


**Figure 6.** Adsorption histogram in successive adsorption–desorption cycles eight times. (Sample: mesoporous CeO<sub>2</sub> powders synthesized hydrothermally at 140 °C for 24 h with 10 mL H<sub>2</sub>O<sub>2</sub>; desorbing agents: 20 mL 0.5 mol/L NaOH; desorption time: 5 min; room temperature).

#### 4. Conclusions

In summary, an oxidation-induced strategy was developed for the template-free hydrothermal synthesis of CeO<sub>2</sub> with a mesoporous structure, in which commercial Ce<sub>2</sub>(CO<sub>3</sub>)<sub>3</sub>•xH<sub>2</sub>O was purchased and served as a cerium precursor, while H<sub>2</sub>O<sub>2</sub> served as an accessible and eco-friendly oxidant employed to achieve the phase transformation of the Ce<sub>2</sub>(CO<sub>3</sub>)<sub>3</sub>•xH<sub>2</sub>O precursor to the CeO<sub>2</sub> phase with a mesoporous structure under the cooperation of following the hydrothermal treatment. H<sub>2</sub>O<sub>2</sub> as an oxidant had a decisive influence on the formation of cubic CeO<sub>2</sub> phase as well as its mesoporous structure; moreover, the values of S<sub>BET</sub>, pore diameters and pore volumes were generally related to the amount of H<sub>2</sub>O<sub>2</sub> in the template-free hydrothermal synthesis. The oxidation-induced and hydrothermal-assisted template-free synthesis of mesoporous CeO<sub>2</sub> can be expected to provide a synthetic alternative for other porous inorganic materials. Preliminary adsorbate evaluation suggested that the as-synthesized mesoporous CeO<sub>2</sub> was a promising absorbent for wastewater treatment containing AO7 dye; the maximum AO7 adsorption efficiency of these mesoporous CeO<sub>2</sub> was found to be 99.8% within 30 min when the initial AO7 concentration was 120 mg/L without the pH preadjustment. The Langmuir isotherm fitted ( $R^2 = 0.9985$ ) the equilibrium data better than the Freundlich isotherm ( $R^2 = 0.9512$ ), with a higher correlation coefficient ( $R^2$ ). The maximum uptake capacity for mesoporous CeO<sub>2</sub> was 757.6 mg/g for AO7 at room temperature according to the Langmuir isotherm model, and it could be easily regenerated by an alkali washing. Moreover, the regeneration experiments revealed the good potential of mesoporous CeO<sub>2</sub> for reuse, even though a slight decrease in adsorption capacity was observed in the subsequent eight cycles.

**Author Contributions:** Y.X. project administration, writing—original draft preparation, data curation, formal analysis; Z.D. funding acquisition, supervision. All authors have read and agreed to the published version of the manuscript.

**Funding:** This study was financially supported by the Leshan Normal University Research Program, China (JPXM2021-18 and 2021SSDJS012), Guiding Project of Scientific Research Program in Ministry of Education of Hubei Province (No. B2021025), and Fundamental Research Funds for the Central Universities (2022CDJXY-010).

**Institutional Review Board Statement:** Not applicable.

**Informed Consent Statement:** Not applicable.

**Data Availability Statement:** Not applicable.

**Conflicts of Interest:** The authors declare no conflict of interest.

## References

1. Waheed, A.; Baig, N.; Ullah, N.; Falath, W. Removal of hazardous dyes, toxic metal ions and organic pollutants from wastewater by using porous hyper-cross-linked polymeric materials: A review of recent advances. *J. Environ. Manag.* **2021**, *287*, 112360. [[CrossRef](#)] [[PubMed](#)]
2. Freeman, H.S.; Reife, A. Dyes, Environmental Chemistry. In *Kirk-Othmer Encyclopedia of Chemical Technology*; John Wiley & Sons, Inc.: Hoboken, NJ, USA, 2003. [[CrossRef](#)]
3. Leulescu, M.; Rotaru, A.; Moanță, A.; Iacobescu, G.; Pălărie, I.; Cioateră, N.; Popescu, M.; Criveanu, M.C.; Morîntale, E.; Bojan, M.; et al. Azorubine: Physical, thermal and bioactive properties of the widely employed food, pharmaceutical and cosmetic red azo dye material. *J. Therm. Anal. Calorim.* **2021**, *143*, 3945–3967. [[CrossRef](#)]
4. Levine, W.G. Metabolism of AZO Dyes: Implication for Detoxication and Activation. *Drug Metab. Rev.* **1991**, *23*, 253–309. [[CrossRef](#)] [[PubMed](#)]
5. Ding, Z.; Li, S.; Zhou, Y.; Chen, Z.; Zhang, F.; Wu, P.; Ma, W. LiBH<sub>4</sub> for hydrogen storage: New perspectives. *Nano Mater. Sci.* **2020**, *2*, 109–119. [[CrossRef](#)]
6. Tanaka, K.; Padermpole, K.; Hisanaga, T. Photocatalytic degradation of commercial azo dyes. *Water Res.* **2000**, *34*, 327–333. [[CrossRef](#)]
7. Ding, Z.; Li, H.; Shaw, L. New insights into the solid-state hydrogen storage of nanostructured LiBH<sub>4</sub>-MgH<sub>2</sub> system. *Chem. Eng. J.* **2019**, *385*, 123856. [[CrossRef](#)]
8. Ding, Z.; Yang, W.; Huo, K.; Shaw, L. Thermodynamics and kinetics tuning of LiBH<sub>4</sub> for hydrogen storage. *Prog. Chem.* **2021**, *33*, 1586–1597. [[CrossRef](#)]
9. Patra, C.; Gupta, R.; Bedadeep, D.; Narayanasamy, S. Surface treated acid-activated carbon for adsorption of anionic azo dyes from single and binary adsorptive systems: A detail insight. *Environ. Pollut.* **2020**, *266*, 115102. [[CrossRef](#)]
10. Kumar, M.; Isloor, A.M.; Todeti, S.R.; Ibrahim, G.P.S.; Inamuddin, I.A.F.; Asiri, A.M. Improved separation of dyes and proteins using membranes made of polyphenylsulfone/cellulose acetate or acetate phthalate. *Environ. Chem. Lett.* **2020**, *18*, 881–887. [[CrossRef](#)]
11. Liu, J.; Huang, S.; Wang, T.; Mei, M.; Chen, S.; Li, J. Peroxydisulfate activation by digestate-derived biochar for azo dye degradation: Mechanism and performance. *Sep. Purif. Technol.* **2021**, *279*, 119687. [[CrossRef](#)]
12. Alderete, B.L.; Silva, J.D.; Godoi, R.; Silva, F.; Picada, J.N. Evaluation of toxicity and mutagenicity of a synthetic effluent containing azo dye after Advanced Oxidation Process treatment. *Chemosphere* **2020**, *263*, 128291. [[CrossRef](#)]
13. Chen, G.; An, X.; Li, H.; Lai, F.; Yuan, E.; Xia, X.; Zhang, Q. Detoxification of azo dye Direct Black G by thermophilic *Anoxybacillus* sp. PDR2 and its application potential in bioremediation. *Ecotox. Environ. Saf.* **2021**, *214*, 112084. [[CrossRef](#)]
14. Ma, M.-L.; Qin, J.-H.; Ji, C.; Xu, H.; Wang, R.; Li, B.-J.; Zang, S.-Q.; Hou, H.-W.; Batten, S.R. Anionic porous metal-organic framework with novel 5-connected vbk topology for rapid adsorption of dyes and tunable white light emission. *J. Mater. Chem. C* **2014**, *2*, 1085–1093. [[CrossRef](#)]
15. Ding, Z.; Lu, Y.; Li, L.; Shaw, L. High Reversible Capacity Hydrogen Storage Through Nano-LiBH<sub>4</sub> + Nano-MgH<sub>2</sub> System. *Energy Storage Mater.* **2019**, *20*, 24–35. [[CrossRef](#)]
16. Hsieh, S.-H.; Manivel, A.; Lee, G.-J.; Wu, J.J. Synthesis of mesoporous Bi<sub>2</sub>O<sub>3</sub>/CeO<sub>2</sub> microsphere for photocatalytic degradation of Orange II dye. *Mater. Res. Bull.* **2013**, *48*, 4174–4180. [[CrossRef](#)]
17. Liu, J.S.; Wang, N.; Zhang, X.F.; Deng, Z.P.; Gao, S. Facile tree leaf-templated synthesis of mesoporous CeO<sub>2</sub> nanosheets for enhanced sensing detection of p-xylene vapors. *J. Alloys Compd.* **2021**, *889*, 161735. [[CrossRef](#)]
18. Shang, Z.; Yang, Z.; Xiao, Y.; Wang, X. Ordered mesoporous Ag/CeO<sub>2</sub> nanocrystalline via silica-templated solution combustion for enhanced photocatalytic performance. *Colloid. Surface. A* **2020**, *604*, 125301. [[CrossRef](#)]
19. Farvardin, N.; Jahani, S.; Kazemipour, M.; Foroughi, M.M. The synthesis and characterization of 3D mesoporous CeO<sub>2</sub> hollow spheres as a modifier for the simultaneous determination of amlodipine, hydrochlorothiazide and valsartan. *Anal. Methods* **2020**, *12*, 1767–1778. [[CrossRef](#)]
20. Jiang, H.; Li, X.; Chen, S.; Wang, H.; Huo, P. g-C<sub>3</sub>N<sub>4</sub> quantum dots-modified mesoporous CeO<sub>2</sub> composite photocatalyst for enhanced CO<sub>2</sub> photoreduction. *J. Mater. Sci.-Mater. Electron.* **2020**, *31*, 20495–20512. [[CrossRef](#)]
21. Fu, X.; Liu, Y.; Deng, J.; Jing, L.; Zhang, X.; Zhang, K.; Han, Z.; Jiang, X.; Dai, H. Intermetallic compound PtMn<sub>y</sub>-derived Pt-MnO<sub>x</sub> supported on mesoporous CeO<sub>2</sub>: Highly efficient catalysts for the combustion of toluene. *Appl. Catal. A-Gen.* **2020**, *595*, 117509. [[CrossRef](#)]
22. Li, W.; Wang, Q.; Wang, L.; Fu, X.; Luo, J. Mesoporous CeO<sub>2</sub>-C hybrid spheres as efficient support for platinum nanoparticles towards methanol electrocatalytic oxidation. *J. Rare Earth.* **2021**, *39*, 674–681. [[CrossRef](#)]
23. Zhao, W.; She, T.; Zhang, J.; Wang, G.; Zhang, S.; Wei, W.; Yang, G.; Zhang, L.; Xia, D.; Cheng, Z.; et al. A novel Z-scheme CeO<sub>2</sub>/g-C<sub>3</sub>N<sub>4</sub> heterojunction photocatalyst for degradation of Bisphenol A and hydrogen evolution and insight of the photocatalysis mechanism. *J. Mater. Sci. Technol.* **2021**, *85*, 18–29. [[CrossRef](#)]
24. Xie, Z.; Zhou, X.; Wu, H.; Zhao, H.; Liu, Y.; Chen, H. One Step Template-Free Synthesis of Mesoporous MnO<sub>x</sub>/CeO<sub>2</sub> Nanocomposite Oxides with Enhanced Low Temperature Catalytic Activity for CO and Hydrocarbon Oxidation. *Catal. Lett.* **2016**, *146*, 1355–1360. [[CrossRef](#)]

25. Liu, X.; Tseng, C.L.; Lin, L.Y.; Lee, C.A.; Li, J.; Feng, L.; Song, L.; Li, X.; He, J.H.; Sakthivel, R.; et al. Template-free synthesis of mesoporous Ce<sub>3</sub>NbO<sub>7</sub>/CeO<sub>2</sub> hollow nanospheres for label-free electrochemical immunosensing of leptin. *Sens. Actuat. B-Chem.* **2021**, *341*, 130005. [[CrossRef](#)]
26. Vikanova, K.; Redina, E.; Kapustin, G.; Nissenbaum, V.; Mishin, I.; Kostyukhin, E.; Kustov, L. Template-free one-step synthesis of micro-mesoporous CeO<sub>2</sub>-ZrO<sub>2</sub> mixed oxides with a high surface area for selective hydrogenation. *Ceram. Int.* **2020**, *46*, 13980–13988. [[CrossRef](#)]
27. Xu, Y.; Li, R. Template-free synthesis of mesoporous CeO<sub>2</sub> powders by integrating bottom-up and top-down routes for acid orange 7 adsorption. *RSC Adv.* **2015**, *5*, 44828–44834. [[CrossRef](#)]
28. Hayashi, Y.; Hosokawa, S.; Imamura, S.; Inoue, M. Pore-Structure-Controlled Coagulates of CeO<sub>2</sub> Nanoparticles for Supporting Ru Catalysts in Liquid Phase Oxidation of Benzyl Alcohol. *J. Ceram. Soc. Jpn* **2007**, *115*, 592–596. [[CrossRef](#)]
29. Wei, Q.; Ma, Q.; Zuo, P.; Fan, H.; Qu, S.; Shen, W. Hollow Structure and Electron Promotion Effect of Mesoporous Pd/CeO<sub>2</sub> Catalyst for Enhanced Catalytic Hydrogenation. *ChemCatChem* **2018**, *10*, 1019–1026. [[CrossRef](#)]
30. Wu, J.; Wang, J.; Du, Y.; Li, H.; Jia, X. Adsorption mechanism and kinetics of azo dye chemicals on oxide nanotubes: A case study using porous CeO<sub>2</sub> nanotubes. *J. Nanopart. Res.* **2016**, *18*, 1–13. [[CrossRef](#)]
31. Xie, A.; Liu, W.; Wang, S.; Liu, X.; Zhang, J.; Yang, Y. Template-free hydrothermal synthesis and CO oxidation properties of flower-like CeO<sub>2</sub> nanostructures. *Mater. Res. Bull.* **2014**, *59*, 18–24. [[CrossRef](#)]
32. Groen, J.C.; Peffer, L.A.A.; Pérez-Ramírez, J. Pore size determination in modified micro- and mesoporous materials. Pitfalls and limitations in gas adsorption data analysis. *Micropor. Mesopor. Mat.* **2003**, *60*, 1–17. [[CrossRef](#)]
33. Fang, J.; Bao, H.; He, B.; Wang, F.; Si, D.; Jiang, Z.; Pan, Z.; Wei, S.; Huang, W. Interfacial and surface structures of CeO<sub>2</sub>-TiO<sub>2</sub> mixed oxides. *J. Phys. Chem. C* **2007**, *111*, 19078–19085. [[CrossRef](#)]
34. Cai, W.; Chen, F.; Shen, X.; Chen, L.; Zhang, J. Enhanced catalytic degradation of AO7 in the CeO<sub>2</sub>-H<sub>2</sub>O<sub>2</sub> system with Fe<sup>3+</sup> doping. *Appl. Catal. B-Environ.* **2010**, *101*, 160–168. [[CrossRef](#)]
35. Ji, P.; Zhang, J.; Chen, F.; Anpo, M. Study of adsorption and degradation of acid orange 7 on the surface of CeO<sub>2</sub> under visible light irradiation. *Appl. Catal. B-Environ.* **2009**, *85*, 148–154. [[CrossRef](#)]
36. Bauer, C.; Jacques, P.; Kalt, A. Investigation of the interaction between a sulfonated azo dye (AO<sub>7</sub>) and a TiO<sub>2</sub> surface. *Chem. Phys. Lett.* **1999**, *307*, 397–406. [[CrossRef](#)]
37. Langmuir, I. The Adsorption of gases on glass, mica and platinum. *J. Am. Chem. Soc.* **1918**, *40*, 1361–1403. [[CrossRef](#)]
38. Freundlich, H. Über die Adsorption in Lösungen. *Z. Phys. Chem.* **1907**, *57U*, 385–470. [[CrossRef](#)]
39. Al-Degs, Y.S.; El-Barghouthi, M.I.; Issa, A.A.; Khraisheh, M.A.; Walker, G.M. Sorption of Zn(II), Pb(II), and Co(II) using natural sorbents: Equilibrium and kinetic studies. *Water Res.* **2006**, *40*, 2645–2658. [[CrossRef](#)]
40. Pedro Silva, J.; Sousa, S.; Rodrigues, J.; Antunes, H.; Porter, J.J.; Gonçalves, I.; Ferreira-Dias, S. Adsorption of acid orange 7 dye in aqueous solutions by spent brewery grains. *Sep. Purif. Technol.* **2004**, *40*, 309–315. [[CrossRef](#)]
41. Hamzeh, Y.; Ashori, A.; Azadeh, E.; Abdulkhani, A. Removal of Acid Orange 7 and Remazol Black 5 reactive dyes from aqueous solutions using a novel biosorbent. *Mat. Sci. Eng. C-Mater* **2012**, *32*, 1394–1400. [[CrossRef](#)]
42. Ashori, A.; Hamzeh, Y.; Ziapour, A. Application of soybean stalk for the removal of hazardous dyes from aqueous solutions. *Polym. Eng. Sci.* **2013**, *54*, 239–245. [[CrossRef](#)]
43. Lin, R.; Liang, Z.; Yang, C.; Zhao, Z.; Cui, F. Selective adsorption of organic pigments on inorganically modified mesoporous biochar and its mechanism based on molecular structure. *J. Colloid Interf. Sci.* **2020**, *573*, 21–30. [[CrossRef](#)]
44. Noorimotlagh, Z.; Darvishi Cheshmeh Soltani, R.; Khataee, A.R.; Shahriyar, S.; Nourmoradi, H. Adsorption of a textile dye in aqueous phase using mesoporous activated carbon prepared from Iranian milk vetch. *J. Taiwan Inst. Chem. E.* **2014**, *45*, 1783–1791. [[CrossRef](#)]
45. Lim, C.K.; Bay, H.H.; Neoh, C.H.; Aris, A.; Abdul Majid, Z.; Ibrahim, Z. Application of zeolite-activated carbon macrocomposite for the adsorption of Acid Orange 7: Isotherm, kinetic and thermodynamic studies. *Environ. Sci. Pollut. Res.* **2013**, *20*, 7243–7255. [[CrossRef](#)]
46. Aber, S.; Daneshvar, N.; Soroureddin, S.M.; Chabok, A.; Asadpour-Zeynali, K. Study of acid orange 7 removal from aqueous solutions by powdered activated carbon and modeling of experimental results by artificial neural network. *Desalination* **2007**, *211*, 87–95. [[CrossRef](#)]
47. Jia, L.; Liu, W.; Cao, J.; Wu, Z.; Yang, C. Modified multi-walled carbon nanotubes assisted foam fractionation for effective removal of acid orange 7 from the dyestuff wastewater. *J. Environ. Manag.* **2020**, *262*, 110260. [[CrossRef](#)]
48. Nourmoradi, H.; Ghiasvand, A.R.; Noorimotlagh, Z. Removal of methylene blue and acid orange 7 from aqueous solutions by activated carbon coated with zinc oxide (ZnO) nanoparticles: Equilibrium, kinetic, and thermodynamic study. *Desalination Water Treat.* **2014**, *55*, 252–262. [[CrossRef](#)]
49. Ghasemi, A.; Shams, M.; Qasemi, M.; Afsharnia, M. Data on efficient removal of acid orange 7 by zeolitic imidazolate framework-8. *Data Brief* **2019**, *23*, 103783. [[CrossRef](#)]
50. Zhou, B.; Tang, Y.; Zhao, L.; Guo, L.; Zhou, J. Novel Fe<sub>3</sub>O<sub>4</sub>-poly(methacryloxyethyltrimethyl ammonium chloride) adsorbent for the ultrafast and efficient removal of anionic dyes. *RSC Adv.* **2021**, *11*, 1172–1181. [[CrossRef](#)]

51. Huo, X.; Zhang, Y.; Zhang, J.; Zhou, P.; Xie, R.; Wei, C.; Liu, Y.; Wang, N. Selective adsorption of anionic dyes from aqueous solution by nickel (II) oxide. *J. Water Supply Res. Technol.* **2019**, *68*, 171–186. [[CrossRef](#)]
52. Li, T.; Liu, Y.; Wang, S.; Zeng, G.; Zheng, B.; Wang, H.; Zhang, M.; Guo, F.; Zeng, X. Synthesis and adsorption application of amine shield-introduced-released porous chitosan hydrogel beads for removal of acid orange 7 from aqueous solutions. *RSC Adv.* **2015**, *5*, 62778–62787. [[CrossRef](#)]